Molecular Cell, Vol. 19, 461–473, August 19, 2005, Copyright ©2005 by Elsevier Inc. DOI 10.1016/j.molcel.2005.06.030

Structural Basis for the Cytoskeletal Association of Bcr-Abl/c-Abl

Oliver Hantschel,[1,2,5] Silke Wiesner,[3,5,7] Thomas Güttler,[4,6] Cameron D. Mackereth,[3,6] Lily L. Remsing Rix,[1,2,6] Zsuzsanna Mikes,[2] Jana Dehne,[2] Dirk Görlich,[4] Michael Sattler,[3,*] and Giulio Superti-Furga[1,2,*]

[1]Center for Molecular Medicine of the Austrian Academy of Sciences
Lazarettgasse 19/3
1090 Vienna
Austria

[2]Developmental Biology Programme

[3]Structural and Computational Biology Programme
European Molecular Biology Laboratory
Meyerhofstrasse 1
69117 Heidelberg
Germany

[4]ZMBH
University of Heidelberg
Im Neuenheimer Feld 282
69120 Heidelberg
Germany

Summary

The Bcr-Abl tyrosine kinase causes different forms of leukemia in humans. Depending on its position within the cell, Bcr-Abl differentially affects cellular growth. However, no structural and molecular details for the anticipated localization determinants are available. We present the NMR structure of the F-actin binding domain (FABD) of Bcr-Abl and its cellular counterpart c-Abl. The FABD forms a compact left-handed four-helix bundle in solution. We show that the nuclear export signal (NES) previously reported in this region is part of the hydrophobic core and nonfunctional in the intact protein. In contrast, we could identify the critical residues of helix αIII that are responsible for F-actin binding and cytoskeletal association. We propose that these interactions represent a major determinant for both Bcr-Abl and c-Abl localization.

Introduction

Expression of Bcr-Abl, the oncogenic counterpart of the tyrosine kinase c-Abl and the outcome of the Philadelphia chromosome translocation (t[9;22]), is the basis for all cases of chronic myelogenous leukemia (CML) and a subset of acute lymphocytic leukemia (ALL) (Wong and Witte, 2004). The predominant distinguishing feature of Bcr-Abl is its high level of tyrosine kinase activity compared to the kinase activity of c-Abl, which is effectively autoinhibited by different intramolecular interactions (Raitano et al., 1997; Hantschel and Superti-Furga, 2004). Inhibition of the tyrosine kinase activity of Bcr-Abl by the small-molecule inhibitor Imatinib/Gleevec has become a paradigm for modern targeted cancer therapy, but emerging cases of drug resistance create a demand for additional therapeutic intervention strategies (Druker, 2004; Sawyers, 2004). Bcr-Abl is predominantly localized to the cytoplasm of cells, where it activates different signal transduction pathways, leading to cell proliferation (McWhirter and Wang, 1991, 1993; Steelman et al., 2004). However, relocalization to the nucleus can be achieved by either combination of pharmacological treatment or genotoxic stress resulting in alteration of its growth-promoting properties (Dierov et al., 2004; Vigneri and Wang, 2001). The cellular form c-Abl localizes to varying degrees to both the cytoplasm and the nucleus depending on tissue type and environmental cues and is thought to shuttle between these two compartments (Van Etten et al., 1989; Wetzler et al., 1993; Renshaw et al., 1988; Taagepera et al., 1998).

Bcr-Abl spans more than 2000 amino acid residues and comprises a complex array of multiple protein-protein interaction and signaling domains, including a centrally located SH3-SH2-tyrosine kinase domain module (Figure 1A). The proposed localization determinants are all found in the C-terminal last exon region that is common to both Bcr-Abl and c-Abl. These include three nuclear localization signals (NLSs) (Wen et al., 1996), a leucine-rich NES (Taagepera et al., 1998), and an FABD (McWhirter and Wang, 1993; Van Etten et al., 1994) (Figure 1A). Although major insight into the regulatory mechanisms of c-Abl autoinhibition could be provided by solving the structure of the SH3-SH2-kinase domain fragment, still only about one-third of Bcr-Abl's protein structure is known to date (Hantschel and Superti-Furga, 2004; Harrison, 2003; Nagar et al., 2003; Hantschel et al., 2003). To explore the molecular basis of Bcr-Abl/c-Abl localization, we solved the structure of the FABD and studied its molecular function. Our data provide structural insights into a localization determinant of Bcr-Abl/c-Abl.

Results and Discussion

NMR Structure of the FABD

We determined the three-dimensional (3D) solution structure of the FABD (corresponding to residues 1026–1149 of human c-Abl spliceform 1b) by heteronuclear NMR spectroscopy (Figures 1B and 1C and Table 1). This domain also includes the previously proposed NES (residues 1109–1118) (Taagepera et al., 1998).

The ordered region of the FABD, which encompasses residues 1047–1149, is a monomer in solution and folds as a compact bundle of four antiparallel α helices, which are arranged in a left-handed topology (Figures 1B and 1C). A predominantly aliphatic core formed by

*Correspondence: gsuperti@cemm.oeaw.ac.at (G.S.-F.); sattler@embl.de (M.S.).

[5]These authors contributed equally to this work.

[6]These authors contributed equally to this work.

[7]Present address: Structural Biology and Biochemistry, Hospital for Sick Children, 555 University Avenue, Toronto, Ontario, M5G 1X8, Canada.

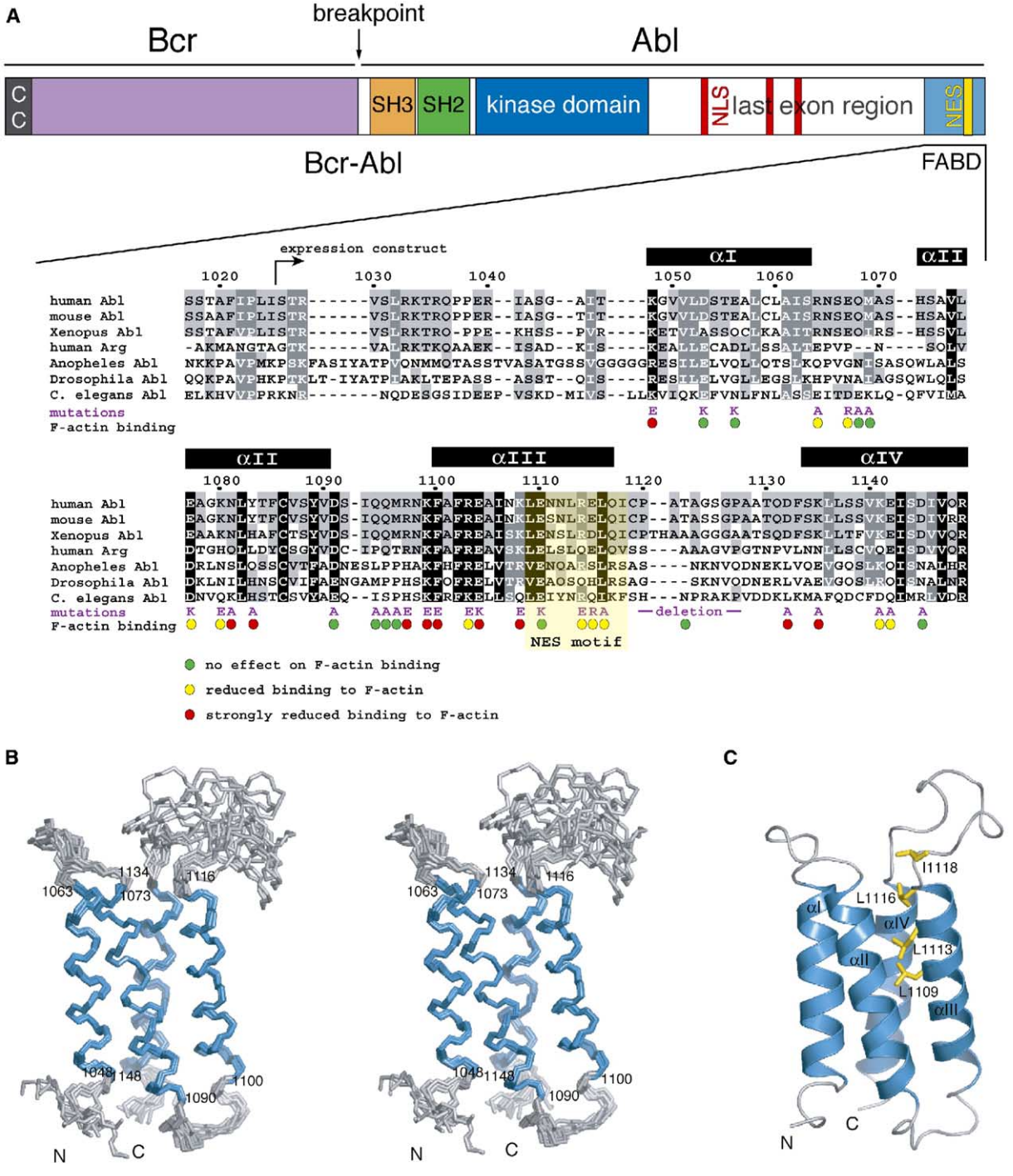

Figure 1. Structure of the Bcr-Abl/c-Abl FABD

(A) Domain architecture of the Bcr-Abl fusion protein (top). Bottom, multiple sequence alignments of Abl FABDs highlighting partial (gray), high (white letters on gray background), and complete (white letters on black background) residue conservation. Sequences of Abl in *Homo sapiens*, *Mus musculus*, *Xenopus laevis*, *Anopheles gambiae*, *Drosophila melanogaster*, *Caenorhabditis elegans*, and of the Abl paralogue Arg (ABL2) in *Homo sapiens* are shown. Residue numbers and secondary structure elements (boxes) are shown on top. The NES and introduced mutations together with results from the F-actin cosedimentation assay are shown on the bottom. Residue numbers correspond to human c-Abl 1b numbering. Abbreviations: CC, coiled-coil domain; SH3, Src-homology 3 domain; SH2, Src-homology 2 domain; NLS, nuclear localization signal; and NES, nuclear export signal.

(B) Stereoview of the ensemble of the ten lowest-energy NMR structures. The backbone trace is shown in gray, whereas secondary structure elements are shown in blue and labeled by residue numbers. Unstructured, N-terminal residues (1026–1039) are omitted for clarity.

(C) Ribbon representation of the lowest energy structure. Secondary structure elements are labeled and shown in blue. The side chains of residues defining the previously proposed NES are shown in yellow.

Table 1. Structural Statistics of the Ten Lowest Energy Structures of the Bcr-Abl/c-Abl FABD

Number of Structural Restraints		
All	2693	
Sequential (|i – j| = 1)	497	
Medium range (2 ≤ |i – j| ≤ 4)	460	
Long range (|i – j| > 4)	369	
Intraresidual	1265	
Unambiguous	2591	
Ambiguous	0	
Hydrogen bonds	102	
Dihedral angles	71 ϕ, 71 ψ, 14 χ_1	
$^1H^N$-^{15}N residual dipolar couplings	64	
Rmsd from Experimental Restraints[a]	<SA>[b]	<SA>$^{water\text{-}refined}$
All distance restraints [Å]	0.027 ± 0.002	0.037 ± 0.002
Unambiguous NOEs [Å]	0.027 ± 0.002	0.037 ± 0.002
Hydrogen bonds [Å]	0.024 ± 0.002	0.025 ± 0.003
Dihedral angles [°]	0.510 ± 0.101	0.518 ± 0.101
RDC Q factor[c]	0.046 ± 0.003	0.058 ± 0.004
Rmsd from Idealized Covalent Geometry		
Bond lengths [Å]	(2.9 ± 0.2) × 10^{-3}	(4.9 ± 0.2) × 10^{-3}
Bond angles [°]	0.468 ± 0.014	0.655 ± 0.017
Improper dihedral angles [°]	0.415 ± 0.028	1.668 ± 0.102
Coordinate Precision[d] [Å]		
Secondary structure elements (N, C^α, C′)	0.33 ± 0.06	0.42 ± 0.08
Secondary structure elements (all heavy atoms)	0.94 ± 0.10	1.03 ± 0.11
Residues 1043–1149 (N, C^α, C′)	1.73 ± 0.45	1.83 ± 0.85
Residues 1043–1149 (all heavy atoms)	2.04 ± 0.35	2.15 ± 0.67
Ramachandran Plot[e] [%]		
Most favored regions (secondary structure elements)	99.7 ± 0.7	99.8 ± 0.5
Additionally allowed regions (secondary structure elements)	0.3 ± 0.7	0.2 ± 0.5
Most favored regions (residues 1043–1149)	77.6 ± 2.5	80.3 ± 2.3
Additionally allowed region (residues 1043–1149)	22.4 ± 2.5	19.7 ± 2.3

[a] In any of the final <SA> structures, no distance restraint was violated by more than 0.4 Å, no dihedral angle restraint was violated by more than 5°, and no residual dipolar coupling restraint was violated by more than 2.5 Hz.
[b] <SA> refers to the ensemble of the ten structures with the lowest energy.
[c] Reference: Cornilescu et al., 1998.
[d] Coordinate precision is given as the pair-wise Cartesian coordinate rmsd of the ten lowest-energy structures.
[e] Excluding glycine and proline residues.

Val1051, Leu1058 (in helix αI), Val1075, Leu1082, Cys1086 (αII), Phe1102, Ala1105, Leu1109, Leu1113 (αIII), Leu1136, Val1140, Ile1143, and Val1147 (αIV) stabilizes this fold. The high degree of conservation of these residues suggests a similar fold for the FABDs of all c-Abl orthologs as well as the c-Abl paralogue Arg (*ABL2*) (Figure 1A). The α helices are connected by long loops that are poorly conserved in length and sequence. ^{15}N relaxation data shows that the αIII-αIV loop displays high internal mobility and that the 20 N-terminal residues of the expression construct are unstructured (Figure S1 available in the Supplemental Data with this article online).

Structural Homologs of the FABD

The structure of the Bcr-Abl/c-Abl FABD is clearly distinct from calponin-homology domains that were recently proposed for the Arg equivalent of the FABD but that bind F-actin only in a tandem configuration (Galkin et al., 2005). Although the Bcr-Abl/c-Abl FABD has no significant sequence similarity to other established F-actin binding domains, the 3D structure exhibits strong homology to domains of other cytoskeletal proteins of which some bind F-actin directly or indirectly: the vinculin head and tail domain (with DALI Z scores [Z] of 9.9 and 8.2, respectively), the dimerization and adhesion modulating domain of α-catenin (Z scores of 9.3 and 9.5, respectively), the vinculin binding domain of talin (Z = 7.9), and the focal adhesion targeting domain of focal adhesion kinase (Z = 7.5) (Figure 2). Sequence homology of these four-helix bundles is limited only to their helical amphipathicity and could not be revealed by simple sequence comparison. Although many proteins include four-helix bundles, the similarity in the interhelical geometry and the unusual left-handed topology between these domains and the Bcr-Abl/c-Abl FABD is intriguing and, besides F-actin binding (see below), may suggest a role in protein complex assembly that is currently not understood in molecular detail (Fillingham et al., 2005). The helix bundle architecture is emerging as a common interaction module in a number of proteins involved in cytoskeletal regulation (Hayashi et al., 2002), pointing at a possible function of Bcr-Abl/c-Abl in the multiprotein complexes anchoring actin filaments. Indeed, cytoplasmic c-Abl colocalizes with many cytoskeletal structures and effectors, thereby

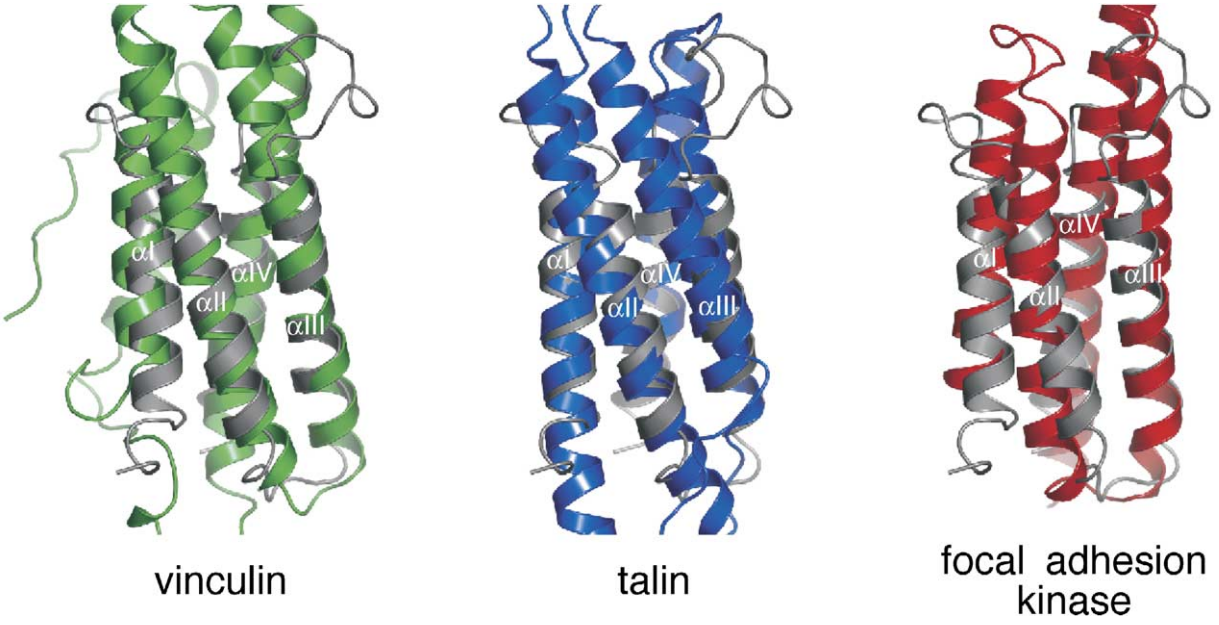

Figure 2. Structural Homologs of the Bcr-Abl/c-Abl FABD

Despite complete absence of sequence similarity, the Bcr-Abl/c-Abl FABD is structurally homologous to domains present in cell adhesion proteins. In all panels, the Bcr-Abl/c-Abl FABD is shown in gray, whereas the vinculin tail domain is displayed in green (left, PDB-entry 1QKR), the vinculin binding domain of talin in blue (middle, PDB-entry 1SJ7), and the focal adhesion targeting domain of focal adhesion kinase in red (right, PDB-entry 1K40).

integrating multiple signals to coordinate F-actin dynamics (Woodring et al., 2003). Previous studies have shown that F-actin binding inhibits c-Abl kinase activity (Woodring et al., 2001). The mechanism by which this occurs is currently unclear but may involve intramolecular interactions between the FABD and other regions of the protein, e.g., the kinase domain. Further structure-function analysis of the FABD should be instrumental in elucidating this regulatory function.

The NES Is Buried and Nonfunctional

Residues comprising the proposed NES (residues 1109–1118) (Taagepera et al., 1998) are located on the αIII helix and the αIII-αIV loop (Figure 1C). Whereas Ile1118 is solvent accessible, Leu1116 is only partially exposed. Both Leu1109 and Leu1113 are buried in the hydrophobic core of the domain. All three leucines (Leu1109, Leu1113, and Leu1116) are involved in an extensive network of hydrophobic interactions with Leu1136 (αIV) and with Leu1076, Gly1079, and Leu1082 (αII).

The fact that most residues of the previously proposed NES (residues 1109–1118) are not solvent exposed raised questions about its physiological relevance. We first investigated whether the isolated NES peptide can form an export complex with the nuclear export receptor CRM1 (exportin 1). The immobilized peptide efficiently recruited CRM1 from a HeLa cell extract, provided RanGTP had been added to mimic a nuclear environment (Figure 3A, lane 7). Leu1116 is essential for NES function of the isolated peptide (Taagepera et al., 1998), and indeed, the L1116A mutation abolishes CRM1 binding (Figure 3A, lane 9). Thus, residues 1109–1118 behave like a leucine-rich NES when presented in isolation. If this NES were also functional in the original domain context, then the FABD should also specifically interact with CRM1. However, CRM1 bound only inefficiently (Figure 3A, lane 3), and crucially, this weak binding was not further reduced by the L1116A mutation (Figure 3A, lane 5). This indicates that the NES is not accessible to CRM1 and that the FABD binds CRM1 only nonspecifically.

Furthermore, immobilized CRM1 specifically bound a green fluorescent protein (GFP)-NES fusion, but not the untagged recombinant FABD, thus excluding the possibility that tagging of the domain or a protein present in the HeLa cell extract had compromised export complex formation (Figure 3B).

To test for nuclear export of the FABD, we performed experiments with HeLa cell nuclei in *Xenopus laevis* egg extract depleted of endogenous nuclear transport receptors (Ribbeck and Gorlich, 2002). The nucleocytoplasmic distribution of added recombinant GFP-FABD and GFP-NES was monitored by confocal microscopy after initial equilibration by diffusion. Upon CRM1 addition, we observed rapid export of GFP-NES, but not of GFP-FABD (Figure 3C). No export occurred when exportin 6 or buffer were added instead of CRM1 (Figure 3C). In agreement with these results, we did not detect export of GFP-FABD or ^{35}S-methionine-labeled full-length c-Abl upon microinjection into the nuclei of frog oocytes (data not shown). Finally, treatment of HeLa or COS cells with the specific CRM1 inhibitor leptomycin B (LMB) did not lead to nuclear accumulation of either endogenous or overexpressed c-Abl (Figure 4 and data not shown). Overall, our results indicate that residues 1109–1118 of Bcr-Abl/c-Abl do not constitute a functional NES in the context of the folded FABD.

Furthermore, as judged from ^{15}N relaxation studies,

the NES does not exhibit internal mobility (Figure S1). Together with the functional data above, this suggests that the NES may not become exposed by a flipping or unfolding mechanism. However, we cannot completely exclude the possibility that under conditions different than the ones tested here, mechanisms may exist that trigger unfolding of the FABD and a release of another functionality, such as the hidden NES motif.

FABD-Dependent Cytoplasmic Localization Pattern

To analyze the precise role of the FABD in the cellular localization of Bcr-Abl and c-Abl, we performed extensive structure-based mutagenesis, careful to minimize general structure perturbation and maximize specific functional effects. We introduced a set of 21 mutants covering 39 solvent-exposed residues (Figure 1A and Table 2) into full-length p210 Bcr-Abl and human c-Abl 1b to perform confocal immunofluorescence microscopy with transiently transfected COS cells. Under the settings used, the low levels of endogenous c-Abl could hardly be detected (data not shown).

Wild-type (wt) Bcr-Abl colocalized with actin filaments, whereas the FABD-deletion mutant failed to do so. Instead, the mutant displayed a diffused localization throughout the cytoplasm with additional punctuated staining, which had previously been observed with other deletion mutants encompassing the same region (McWhirter and Wang, 1993) (Figure 5A and data not shown). Localization patterns of the different Bcr-Abl FABD point mutants fell between that of the wt protein and that of the FABD-deletion mutant (Table 2). Three mutations, R1097E, K1099E, and F1100E, showed the Bcr-Abl localization phenotype most similar to the FABD-deletion mutant (F1100E shown in Figure 5A). The punctuate staining seemed to depend on kinase activity, as cells treated with the kinase inhibitor Imatinib/Gleevec did not show this phenotype (Figure S2).

Differences in actin colocalization between wt and mutant proteins of c-Abl were less evident but still readily detectable (Figure 5B). Mutants that showed the strongest defect in association with actin filaments were the same for both Bcr-Abl and c-Abl. Interestingly, some of these c-Abl FABD mutants showed a partial or strong nuclear localization (Table 2 and Figure 5B), such as F1100E and the L1116A mutation of the previously proposed NES.

The F-Actin Binding Site

To establish the precise molecular nature of the FABD-dependent localization properties of Bcr-Abl/c-Abl described above, we performed a quantitative analysis of the ability of the recombinant FABD wt and mutants to bind purified F-actin in vitro. All FABD proteins were expressed as GST-fusions, purified to homogeneity, and tested in an F-actin cosedimentation assay (Figure S3A). Structural integrity was assessed by using gel filtration chromatography, NMR, and far-ultraviolet circular dichroism spectroscopy (for selected mutants, see Figures S3B-S3D and data not shown). Although GST-FABD wt was enriched in the pellet in the presence of F-actin, only a minor proportion was found in the pellet fraction in the absence of F-actin (Figure 6A, top). This suggests specific binding to F-actin in vitro. The FABD mutants were tested accordingly and compared to the wt protein (Table 2). Mutation of Arg1097, Lys1099, Phe1100, and Glu1104/Lys1108 impaired F-actin binding strongest (Table 2 and Figures 1A, 6A, and 6B). Importantly, mutation of residues within the previously proposed NES (Leu1116, Arg1114, and Glu1115) led to an intermediate reduction in F-actin binding (Table 2). Independently, NMR titration experiments with ^{15}N-labeled FABD and F-actin showed a general line-broadening effect depending on the F-actin concentration consistent with the formation of a high-molecular weight complex (Figure S4). Although for some domains structurally related to the FABD a potential to undergo dramatic conformational changes upon ligand binding has been observed, we have not observed any major chemical shift changes in our NMR titrations that might indicate such a behavior for the Bcr-Abl/c-Abl FABD.

Color coding of the surface of the FABD according to the contribution of the residues to F-actin binding revealed a cluster of residues along helix αIII, including the previously proposed NES, as well as adjacent portions of helix αII and helix αIV (Figure 6B). Independently, analysis of evolutionary conservation among Abl FABDs showed that, in contrast to most of the solvent-exposed residues, residues in the N-terminal half of αIII are highly conserved (Figure 6C). The fact that the only highly conserved region of the domain coincides with the F-actin binding epitope suggests that F-actin binding is the key conserved function among the various Abl FABDs.

To visualize how the evolutionarily conserved helix αIII could possibly interact with F-actin, we generated models of the Bcr-Abl/c-Abl FABD-actin complex with the program HADDOCK (Dominguez et al., 2003) using an ensemble of seven NMR structures of the Abl FABD and actin coordinates from four different actin complexes. Although the residues in actin involved in binding the FABD could not be determined experimentally, crystal structures of actin complexes reveal a hydrophobic cleft between actin subdomains 1 and 3 (Figure S5A) as the primary interaction site for F-actin binding proteins (Dominguez, 2004; Aguda et al., 2005). By superimposing structures of four actin complexes, 19 residues in and surrounding this hydrophobic cleft were chosen to generate docking restraints. Indeed, the conserved helix αIII could be docked reliably onto a hydrophobic cleft in the actin structure. It is worth noting that this binding mode would be compatible with the simultaneous actin-actin interactions within F-actin as predicted in the Holmes model (Holmes et al., 1990) (Figure S5).

Molecular Basis for the NES Phenotype

Leucine-rich NESs consist of a stretch of regularly spaced hydrophobic residues, an abundant sequence motif, and an intrinsic feature of amphipathic helices. Previous studies have led to the widely acknowledged view that c-Abl and Bcr-Abl possess a functional NES at the C terminus (Taagepera et al., 1998; Wang, 2000; Henderson and Eleftheriou, 2000; Zhu and Wang, 2004). Several key experiments that led to this perception, however, were performed with the NES as a peptide or with constructs that inadvertently affected the FABD structural integrity. Unfolding of the FABD had two consequences. On one hand, normally buried elements of

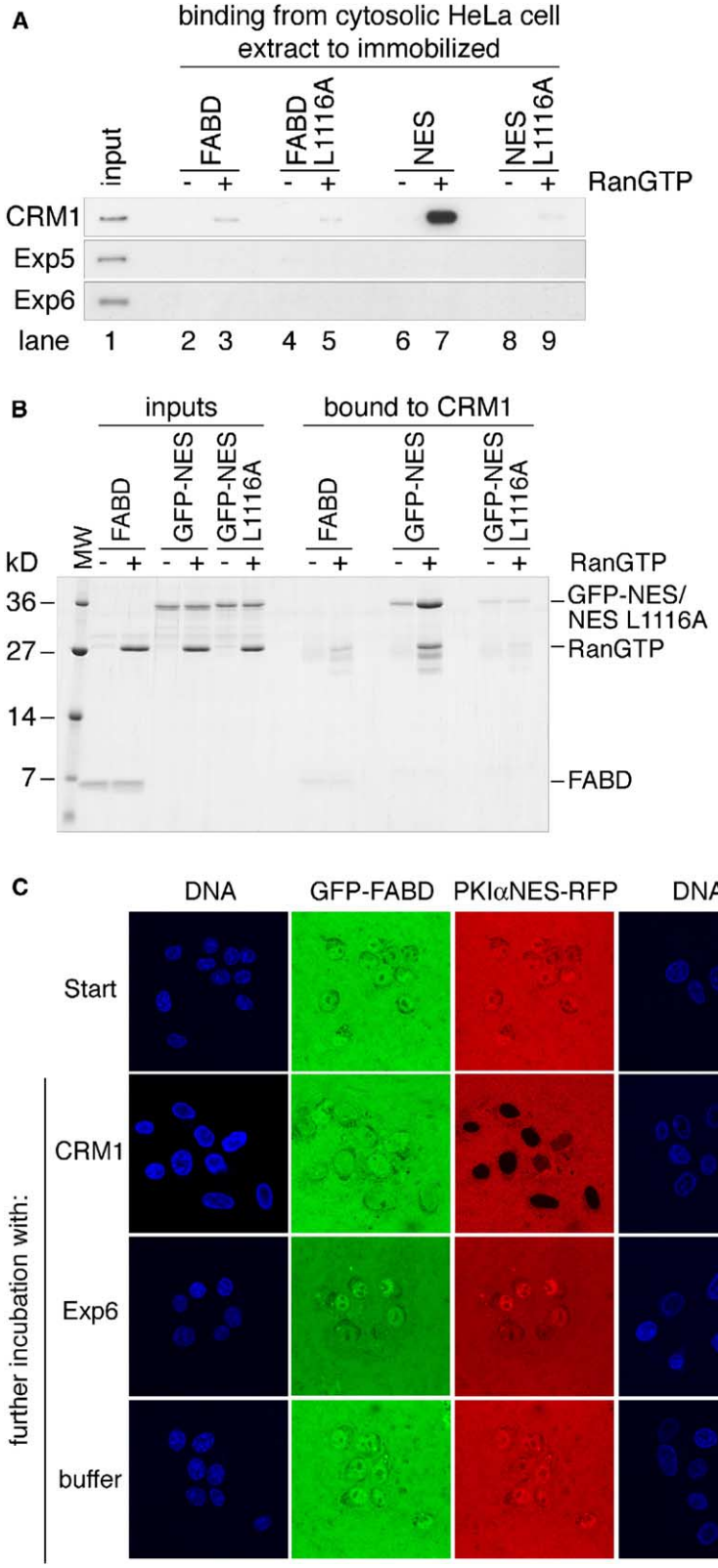

Figure 3. The Folded FABD Does Not Bind to CRM1 and Is Not Exported from the Nucleus

(A) FABD, NES$^{1109–1118}$, and the respective L1116A mutants were immobilized on a Sepharose resin in equimolar amounts and allowed to bind exportins from a HeLa cell extract. RanGTP was used to mimic a nuclear environment. Starting material and bound fractions were analyzed by SDS-PAGE and immunoblotting. Exportin 5 (Exp5) and exportin 6 (Exp6) are included as specificity controls. Load in the bound fractions corresponds to 60 times the starting material.

the hydrophobic core became solvent accessible and thereby established a functional, but nevertheless nonphysiological CRM1 binding site. On the other hand, the disrupted domain could no longer bind F-actin. In all these cases, subcellular localization is affected in consequence. As we have shown above, the classic Abl "NES$^-$" mutation L1116A causes impaired F-actin binding, thereby leading to nuclear accumulation indirectly. This case is consistent with the general notion that mutation of linear motifs of proteins in the absence of 3D structural information can be difficult to interpret (Puntervoll et al., 2003). As shown for the nonsense-mediated mRNA decay factor UPF3b (Kadlec et al., 2004), we predict that once structural information becomes available, several other NESs that have been proposed based only on the amino acid sequence will also be revealed to be just nonfunctional, buried hydrophobic core residues.

Conclusion

Taken together, our data strongly suggest that an equilibrium between nuclear import and FABD-dependent cytoplasmic retention determines the subcellular distribution of c-Abl. In support of this, caspase cleavage of c-Abl causes removal of the FABD and leads to nuclear localization and contributes to the induction of apoptosis (Barilá et al., 2003).

The c-Abl and Bcr-Abl proteins share most of their sequences, and indeed, evidence that many of the intramolecular regulatory mechanisms that inhibit c-Abl kinase activity are also operational in Bcr-Abl has emerged recently (Azam et al., 2003; Smith et al., 2003; Hantschel and Superti-Furga, 2004). The Bcr moiety, unique to Bcr-Abl, contributes a coiled-coil oligomerization function that results in proximity-induced *trans*-phosphorylation of the activation loop and consequent high levels of kinase activity (McWhirter et al., 1993; Zhang et al., 2001). We also propose here that the subcellular localization of these two proteins is subject to the same basic mechanisms. But why is mutation of the FABD of Bcr-Abl, in contrast to c-Abl, not sufficient to cause relocalization of the protein from the actin cytoskeleton to the nucleus? In our hands, treatment with the kinase inhibitor Imatinib/Gleevec, although changing the pattern of cytoplasmic staining, did not lead to nuclear localization of FABD-deficient forms of Bcr-Abl, thus excluding a predominant role of kinase activity in cytoplasmic retention (Figure S2). However, preliminary experiments with forms of Bcr-Abl mutated in the coiled-coil domain, in addition to a disrupting mutation in the FABD domain, showed a weak but reproducible nuclear staining (data not shown). This suggests that interaction of Bcr-Abl with the cytoskeleton through the FABD as well as oligomerization contribute to offset any nuclear localization force acting on the protein. Moreover, recent evidence suggests that nuclear import of c-Abl can be inhibited by phosphorylation of a threonine residue (Yoshida et al., 2005). This mechanism might also account for inhibition of nuclear entry of Bcr-Abl.

Irrespective of what precise subcellular distribution may result from actin binding deficiency of Bcr-Abl under different conditions, there appear to be important functional consequences. It has been reported that deletions disrupting FABD integrity impaired both the transforming potential of Bcr-Abl in rat fibroblasts as well as oncogenicity in transgenic mice (McWhirter and Wang, 1993; Heisterkamp et al., 2000). Because we could confine the critical elements of association with the actin cytoskeleton to the N-terminal half of the helix αIII on Bcr-Abl, it might be possible to interfere with this interaction pharmacologically, thus modulating the biological activity of Bcr-Abl. Such intervention may be complementary to targeting of the ATP binding or substrate binding pocket.

Experimental Procedures

Bacterial Expression Constructs

A pETM30 vector (modified pET24d [Novagen] provides an N-hexaHis-GST-tag, followed by a TEV-protease cleavage site) was used for NMR-sample preparation and F-actin cosedimentation assays. For binding and nuclear export assays, two derivatives of the pQE vectors (Qiagen) were used, one providing an N-decaHis-zz-TEV-tag and the other an N-decaHis-EGFP-tag. The coding region of the F-actin binding domain (residues 1026–1149, human c-Abl spliceform 1b numbering) of human Bcr-Abl/c-Abl was cloned into the vectors described above by using standard molecular cloning techniques.

Protein Expression and Purification

For NMR studies, uniformly ^{15}N- and ^{15}N,^{13}C-labeled hexaHis-GST-FABD was expressed as described (Wiesner et al., 2005).

All other proteins were expressed in *E. coli* BLR and purified on Ni-NTA-agarose. Untagged FABD was generated by TEV-protease cleavage of decaHis-zz-FABD, and removal of the tag was via Ni-NTA-agarose. Expression and purification of zz-CRM1-His, His-CRM1, His-Ran(Q69L)GTP, PKIα-NES-mRFP-His, and His-Exp6 has been described previously (Stuven et al., 2003).

Structure Determination

NMR spectra were recorded at 295 K on Bruker DRX 500, 600, and 900 spectrometers, processed with the NMRPipe/NMRDraw package, and analyzed with XEASY. ^{15}N relaxation data were analyzed by using NMRView. ^{1}H, ^{13}C, and ^{15}N chemical shifts were assigned by standard triple-resonance experiments as described (Wiesner et al., 2005).

Proton-proton distance restraints were derived from 3D ^{15}N- and ^{13}C-edited NOE experiments. Dihedral angle restraints for the backbone angles ϕ were determined from quantitative $^{3}J(H^{N},H^{\alpha})$-correlation experiments (Kubinowa et al., 1994), whereas additional

(B) CRM1 was immobilized as above, and recombinant FABD, GFP-NES$^{1109–1118}$, and GFP-NES L1116A were allowed to bind to CRM1 in the absence or presence of RanGTP. Analysis of starting material and bound fractions was by SDS-PAGE and Coomassie staining. Load in the bound fractions corresponds to 40 times the starting material.

(C) HeLa cell nuclei were incubated in a *Xenopus laevis* egg extract, which had been depleted of endogenous nuclear transport receptors. GFP-FABD or GFP-NES was added and allowed to enter the nuclei ("start"). The NES of the inhibitor of protein kinase A fused to red fluorescent protein (PKIαNES-RFP) was used as an internal positive control. The samples were then split and either CRM1, exportin 6, or buffer added. 20 min later, the distribution of the fluorescent proteins was imaged by confocal laser scanning microscopy. DNA staining with DAPI highlights nuclei.

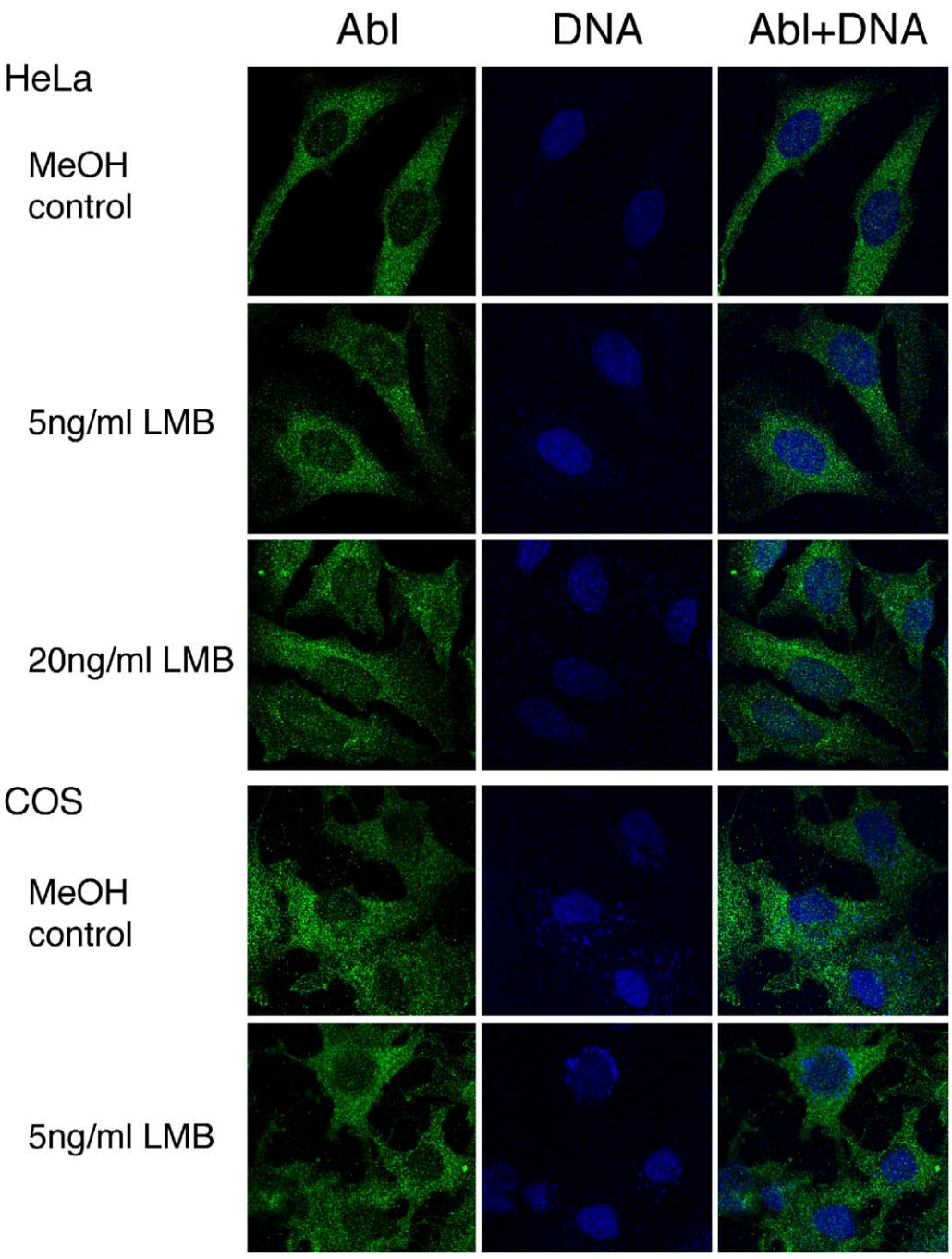

Figure 4. LMB Treatment Does Not Increase Nuclear Levels of c-Abl

Endogenous c-Abl-expressing HeLa and COS cells were treated with 5 ng/mL and/or 20 ng/mL LMB for 4 hr. Cells were fixed and immunostained with anti-Abl antibody (Abl). Nuclei (DNA) were stained with DRAQ5.

ϕ and ψ restraints were derived from TALOS (Cornilescu et al., 1999). $^{3}J(N,C')$ coupling constants were measured by using spin-echo difference experiments to restrain the side-chain angle χ_1 to 180° ± 40° and 0° ± 90°, respectively (Hu and Bax, 1997). $^{1}H,^{15}N$-residual dipolar couplings were measured in ether/alcohol liquid crystalline phase (Ruckert and Otting, 2000) by using a 2D spin-state-selective coherence transfer HSQC experiment (Lerche et al., 1999). Axial and rhombic components of the alignment tensor were –8.5 Hz and –3.6 Hz, respectively. Hydrogen bond restraints were applied as indicated by $^{3}J(H^{N},H^{\alpha})$ constants, $^{13}C^{\alpha}$ and $^{13}C^{\beta}$ secondary chemical shifts, H/D amide exchange rates, and NOE patterns. For structure calculation, the experimentally determined restraints were applied in a mixed torsion, and Cartesian angle dynamics simulated annealing protocol by using CNS (Brunger et al., 1998) and ARIA 1.2 (Nilges and O'Donoghue, 1998). Structures were calculated in eight iterations producing 20 structures in each of the first seven iterations and 50 structures in the final iteration. The quality of the ten lowest energy structures was analyzed by using the programs CNS and PROCHECK-NMR (Laskowski et al., 1996). Table 1 summarizes the structural statistics for the ensemble of the

Table 2. Mapping of the F-Actin Binding Site of the FABD

		F-Action Binding	Localization		
		GST-FABD[a]	Bcr-Abl[b]	c-Abl[c]	
Structural Location	Mutation	In Vitro Binding	Actin Colocalization	Cytoplasm-Nucleus	Actin Colocalization
	wt	1.00	wt	C	A
	ΔFABD	–	p	C/N	a
αI	K1048E	0.61	wt	C	a
αI	D1053K/E1056K	1.05	wt	C	A
αI	R1064A/E1067R	0.92	wt	C	A
L I-II	E1067A/Q1068A/M1069A	1.20	wt	C	A
αII	E1077K/K1080E	0.85	wt	C/N	a
αII	N1081A/Y1083A	0.59	wt	C	A
αII	D1091A	1.03	wt	Not tested	Not tested
L II-III	Q1094A/Q1095A/M1096A	1.21	Not tested	C	A
L II-III	R1097E	0.41	p	C/N	a
αIII	K1099E	0.51	p	C	a
αIII	F1100E	0.41	p	N	a
αIII	R1103E	0.70	p	C	a
αIII	E1104K/K1108E	0.55	p	C/N	A
αIII	E1110K	1.17	i	C/N	a
αIII	R1114E/E1115R	0.91	wt	C	A
αIII	L1116A	0.73	wt	N	A
L III-IV	ΔP1120-P1127	1.17	wt	C	A
αIV	D1132A/K1135A	0.66	wt	C	A
αIV	K1141A/E1142A	0.76	wt	C/N	A
αIV	D1145A	1.00	wt	C/N	a

[a] GST-FABD: relative values for F-actin binding in cosedimentation assays.
[b] Bcr-Abl: wt, F-actin colocalization; i, intermediate; and p, punctuate staining (reduced binding).
[c] c-Abl: C, cytoplasmic; C/N, intermediate localization; N, nuclear; A, F-actin colocalization; and a, reduced F-actin colocalization.

ten lowest energy structures. Figures of 3D structures and molecular surface representations were prepared by using PyMol (DeLano, 2002).

NMR Titration and ^{15}N Relaxation Studies

For NMR titrations, ^{1}H,^{15}N-HSQC experiments were recorded on a 500 MHz spectrometer fitted with a cryoprobe. ^{15}N-labeled FABD was dissolved in 5 mM Tris-HCl (pH 8.0), 50 mM KCl, 0.2 mM $CaCl_2$, 1 mM ATP, 0.5 mM DTT, and 10% $^{2}H_2O$ at an initial protein concentration of 30 μM. The sample was titrated at 295 K with freshly polymerized F-actin (Cytoskeleton, Inc.) prepared in the same buffer as described above, toward a final sample containing 1.2 molar equivalents F-actin (based on the monomeric actin concentration) equal to 15 μM and 18 μM of FABD and F-actin, respectively. Backbone amide ^{15}N relaxation parameters were acquired as described (Wiesner et al., 2005).

Protein-Protein Docking Simulations

Structural models of the Bcr-Abl/c-Abl FABD-actin complex were generated with the program HADDOCK by using standard protocols and parameters (Dominguez et al., 2003). A set of 20 ambiguous interaction restraints (AIRs) was defined for the Bcr-Abl/c-Abl FABD based on the results of the F-actin cosedimentation assays. Although we could not experimentally determine the actin residues involved in binding the FABD, analysis of crystal structures of actin complexes reveals a hydrophobic cleft between actin subdomains 1 and 3 as the primary interaction site for F-actin binding proteins (Dominguez, 2004; Aguda et al., 2005). Residues in and surrounding this hydrophobic cleft were chosen for docking from a superposition of known structures of actin complexes. This resulted in 19 AIRs for the actin monomer. An ensemble of seven NMR structures of the Bcr-Abl/c-Abl FABD and actin coordinates from four actin complexes (PDB-entries: 1EQY, 1SQK, 1QZ5, and 1KXP) were used as input structures for initial rigid-body docking. From the resulting 500 energy-minimized structures, 50 were chosen based on AIR restraint energy and subjected to semiflexible simulated annealing followed by a final refinement in explicit water. Among the final water-refined ten lowest energy structures, eight models adopted conformations as shown in Figure S5 with a pair-wise backbone rmsd of 1.8 ± 0.8 Å, whereas the orientation of the FABD was inverted with respect to the orientation shown in Figure S5 in the remaining two models.

Binding Assays

For the binding experiment of Figure 3A, zz-tagged FABD, NES, and the respective L1116A mutants were immobilized on IgG-Sepharose. The beads were incubated with HeLa cell extract in the presence of an energy-regenerating system (Kutay et al., 1997) and 30 μM cytochalasin B. A nuclear environment was mimicked by addition of GTPase-deficient Ran mutant (Ran[Q69L]GTP) (Klebe et al., 1995). Unbound material was removed, and the beads were washed with 10 ml of binding buffer. Bound proteins were eluted with SDS-sample buffer and analyzed by SDS-PAGE followed by Western blotting. Antibodies against CRM1, Exp5, and Exp6 have been described previously (Mingot et al., 2004; Stuven et al., 2003). For Figure 3B, recombinant FABD (3 μM), GFP-$NES^{1109–1118}$, or GFP-NES L1116A (both 1 μM) were allowed to bind to immobilized human CRM1 in the presence or absence of Ran(Q69L)GTP. Bound proteins were eluted with 50 mM Tris (pH 7.5), 1.5 M $MgCl_2$, isopropanol precipitated, separated by SDS-PAGE, and analyzed by Coomassie staining.

In Vitro Nuclear Export

Xenopus leavis egg extract and HeLa cell nuclei were prepared as described (Stuven et al., 2003). Nuclei were mixed with egg extract depleted of nuclear transport receptors and replenished with Ran, NTF2, and an energy-regenerating system (Ribbeck and Gorlich, 2002). GFP-FABD (residues 1039–1149), GFP-$NES^{1109–1118}$, and mRFP-PKIαNES were used at 2 μM. Exportins were added after 20 min of nucleocytoplasmic equilibration at 1 μM.

Mammalian Expression Constructs

p210 Bcr-Abl was kindly provided by Martin Ruthardt (Johann Wolfgang Goethe-University, Frankfurt, Germany). pSGT vector and pSGT-Abl constructs were previously described (Barilá and Superti-Furga, 1998). The ΔFABD mutation was performed as pre-

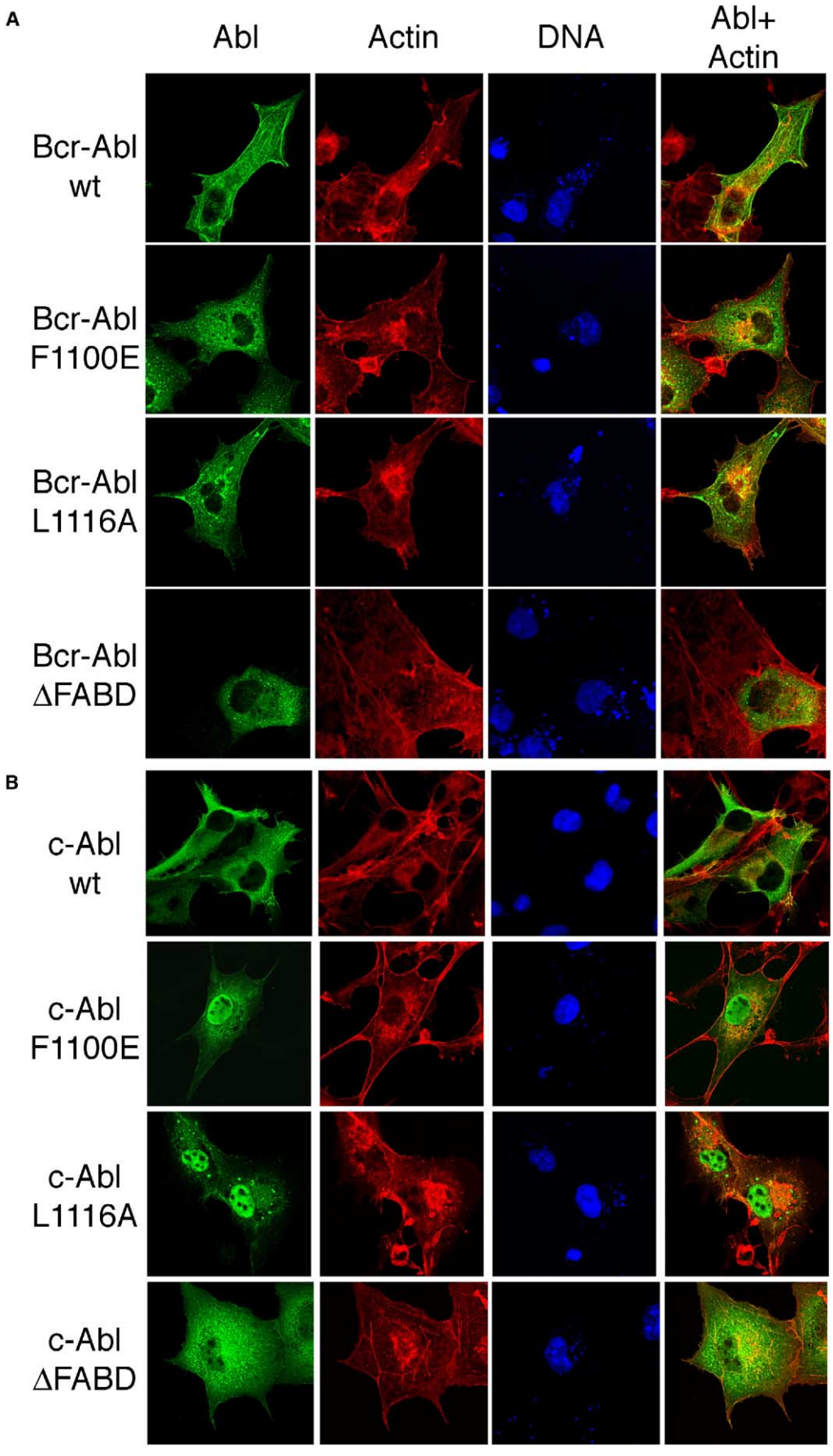
A
Abl
Actin
DNA
Abl+
Actin
Bcr-Abl
wt
Bcr-Abl
F1100E
Bcr-Abl
L1116A
Bcr-Abl
ΔFABD
B
c-Abl
wt
c-Abl
F1100E
c-Abl
L1116A
c-Abl
ΔFABD

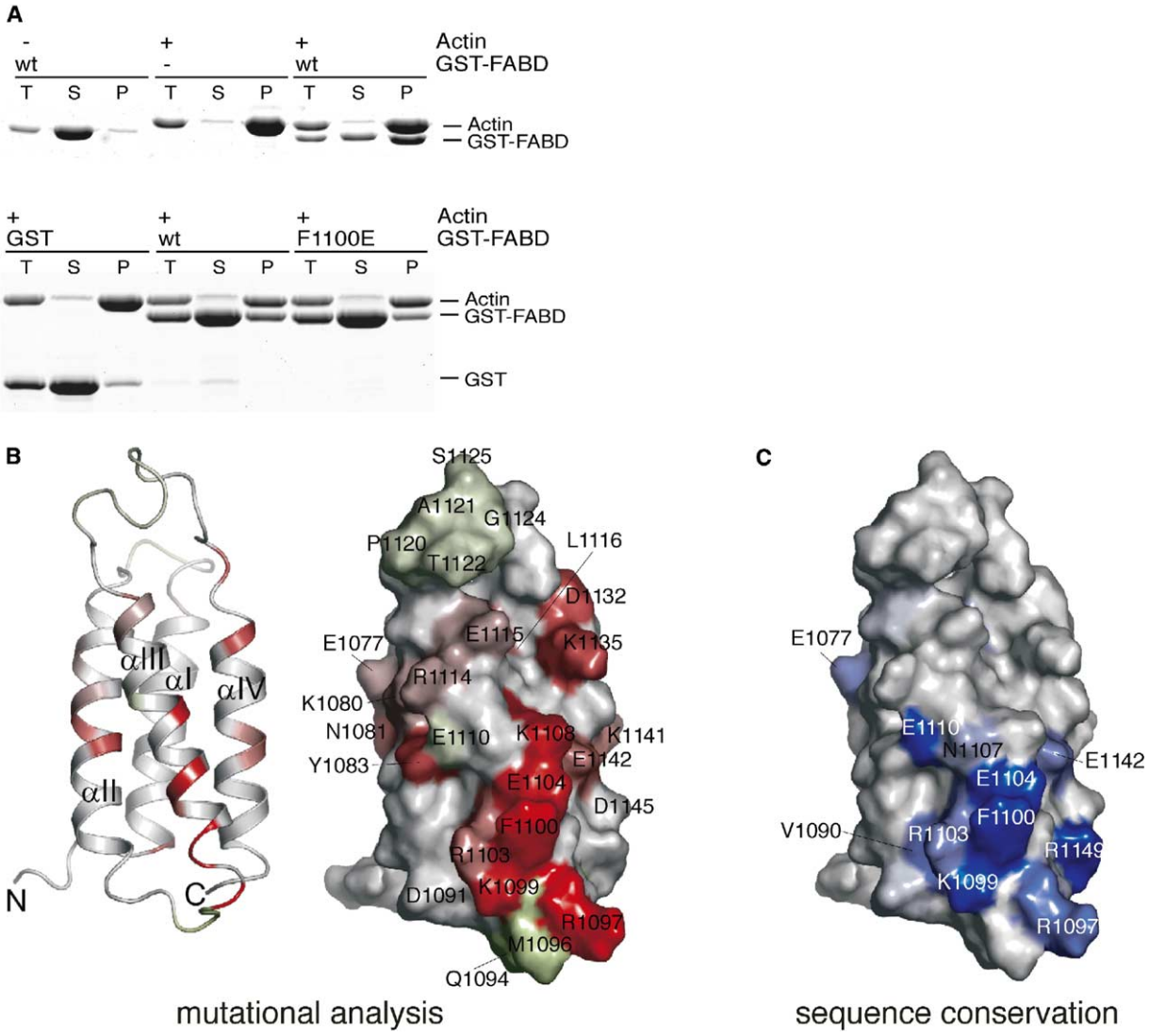

Figure 6. Mutational Analysis of the Bcr-Abl/c-Abl F-Actin Binding Domain

(A) F-actin cosedimentation assay: the indicated proteins were incubated for 30 min and spun at 135,000 × g. 10% of the total reaction before centrifugation (T) and equal amounts of the supernatant (S) and pellet (P) were resolved by SDS-PAGE, stained with Coomassie, and quantified by using the LI-COR Odyssey system.

(B) Ribbon and surface representation of the FABD highlighting effects of individual mutations on F-actin binding activity (see Table 2). Residues are colored with a linear gradient from red to white to green (red, 60% relative inhibition; green, 20% relative enhanced binding activity). All other residues are shown in white.

(C) Surface representation of the FABD highlighting sequence conservation. High to low sequence conservation is colored from blue to white, respectively. In all panels, the FABD is shown in the same orientation.

viously described (Woodring et al., 2001). All mutations were obtained by using the QuikChange Site-Directed Mutagenesis Kit (Stratagene). All mutations were confirmed by sequencing.

Immunofluorescence

COS cells were transfected with either pSG-p210, pSGT-Abl, or mutants thereof by using PolyFect Transfection Reagent (Qiagen). After 24–48 hr of incubation, cells were washed with PBS and fixed with 3% para-formaldehyde. Cells were permeabilized with 0.5% Triton X-100 and blocked with 2.5% normal goat serum (Jackson ImmunoResearch). To visualize Bcr-Abl/c-Abl, primary (rabbit anti-Abl, K12; Santa Cruz) and secondary (anti-rabbit AlexaFluor488; Molecular Probes) antibodies were diluted in blocking solution and incubated with the cells at room temperature. F-actin and nuclei

Figure 5. Localization of Bcr-Abl/c-Abl FABD Mutant Proteins

COS cells were transiently transfected with the indicated (A) Bcr-Abl or (B) c-Abl expression constructs. Cells were fixed and immunostained with anti-Abl antibody (Abl). F-actin (Actin) and nuclei (DNA) were stained with rhodamine-conjugated phalloidin and DRAQ5, respectively.

were stained with rhodamine-conjugated phalloidin (Molecular Probes) and DRAQ5 (Biostatus Limited), respectively. Treatment with STI571/Gleevec was done for 4 hr at 20 μM. Images were obtained on a Zeiss LSM510 confocal microscope by using a 40×/1.3 Plan Neofluar objective.

F-Actin Cosedimentation Assays

GST-FABD fusion proteins were expressed in pETM30 and purified as described (Wiesner et al., 2005) with the exception that the TEV cleavage step was omitted. The fusion proteins were concentrated (15–25 mg/ml). Rabbit muscle actin (Cytoskeleton Inc.) was polymerized according to the manufacturer's instructions. Centrifugations were performed in a Beckman TLS-55 rotor at 135,000 × g. GST-FABD proteins were incubated with equimolar amounts of F-actin in a final volume of 50 μl. 5 μl of the reaction mixture was removed before ultracentrifugation ("total" sample). After ultracentrifugation, the supernatant was removed and the pellet resuspended in SDS-PAGE sample buffer. The "total" sample and equivalent amounts of supernatant and pellet (1/3 of the total reaction) were separated by SDS-PAGE followed by Coomassie staining and quantification using the LI-COR Odyssey system. Levels of F-actin binding in Table 2 were expressed relative to the wt protein.

Supplemental Data

Supplemental Data include Supplemental References and five figures and are available with this article online at http://www.molecule.org/cgi/content/full/19/4/461/DC1/.

Acknowledgments

We thank the Frankfurt DFG/NMR 900 MHz center; the European Molecular Biology Laboratory (EMBL)/Heidelberg and Institute of Molecular Pathology/Vienna confocal microscopy facilities; G. Stier for advice; M. Way, K. Djinovic-Carugo, and V. Small for reading of the manuscript; and K. Dorey for the *Xenopus* sequence. This work was supported by fellowships from the EMBL (O.H.), European Molecular Biology Organization (C.D.M.), German Research Foundation DFG (S.W.), Aventis (O.H.), Boehringer Ingelheim Fonds (T.G.), and the Leukemia and Lymphoma Society (L.L.R.R.). Work in the participating labs is funded by the EMBL, the Austrian Academy of Sciences, and the DFG.

Received: April 15, 2005
Revised: June 2, 2005
Accepted: June 22, 2005
Published: August 18, 2005

References

Aguda, A.H., Burtnick, L.D., and Robinson, R.C. (2005). The state of the filament. EMBO Rep. *6*, 220–226.

Azam, M., Latek, R.R., and Daley, G.Q. (2003). Mechanisms of autoinhibition and STI-571/imatinib resistance revealed by mutagenesis of BCR-ABL. Cell *112*, 831–843.

Barilá, D., and Superti-Furga, G. (1998). An intramolecular SH3-domain interaction regulates c-Abl activity. Nat. Genet. *18*, 280–282.

Barilá, D., Rufini, A., Condo, I., Ventura, N., Dorey, K., Superti-Furga, G., and Testi, R. (2003). Caspase-dependent cleavage of c-Abl contributes to apoptosis. Mol. Cell. Biol. *23*, 2790–2799.

Brunger, A.T., Adams, P.D., Clore, G.M., DeLano, W.L., Gros, P., Grosse-Kunstleve, R.W., Jiang, J.S., Kuszewski, J., Nilges, M., Pannu, N.S., et al. (1998). Crystallography & NMR system: a new software suite for macromolecular structure determination. Acta Crystallogr. D Biol. Crystallogr. *54*, 905–921.

Cornilescu, G., Marquardt, J.L., Ottiger, M., and Bax, A. (1998). Validation of protein structure from anisotropic carbonyl chemical shifts in a dilute liquid crystalline phase. J. Am. Chem. Soc. *120*, 6836–6837.

Cornilescu, G., Delaglio, F., and Bax, A. (1999). Protein backbone angle restraints from searching a database for protein chemical shifts and sequence homology. J. Biomol. NMR *13*, 289–302.

DeLano, W.L. (2002). The PyMOL Molecular Graphics System. http://pymol.sourceforge.net.

Dierov, J., Dierova, R., and Carroll, M. (2004). BCR/ABL translocates to the nucleus and disrupts an ATR-dependent intra-S phase checkpoint. Cancer Cell *5*, 275–285.

Dominguez, C., Boelens, R., and Bonvin, A.M.J.J. (2003). HADDOCK: a protein-protein docking approach based on biochemical or biophysical information. J. Am. Chem. Soc. *125*, 1731–1737.

Dominguez, R. (2004). Actin-binding proteins--a unifying hypothesis. Trends Biochem. Sci. *29*, 572–578.

Druker, B.J. (2004). Imatinib as a paradigm of targeted therapies. Adv. Cancer Res. *91*, 1–30.

Fillingham, I., Gingras, A.R., Papagrigoriou, E., Patel, B., Emsley, J., Critchley, D.R., Roberts, G.C., and Barsukov, I.L. (2005). A vinculin binding domain from the talin rod unfolds to form a complex with the vinculin head. Structure (Camb) *13*, 65–74.

Galkin, V.E., Orlova, A., Koleske, A.J., and Egelman, E.H. (2005). The Arg non-receptor tyrosine kinase modifies F-actin structure. J. Mol. Biol. *346*, 565–575.

Hantschel, O., and Superti-Furga, G. (2004). Regulation of the c-Abl and Bcr-Abl tyrosine kinases. Nat. Rev. Mol. Cell Biol. *5*, 33–44.

Hantschel, O., Nagar, B., Guettler, S., Kretzschmar, J., Dorey, K., Kuriyan, J., and Superti-Furga, G. (2003). A myristoyl/phosphotyrosine switch regulates c-Abl. Cell *112*, 845–857.

Harrison, S.C. (2003). Variation on an Src-like Theme. Cell *112*, 737–740.

Hayashi, I., Vuori, K., and Liddington, R.C. (2002). The focal adhesion targeting (FAT) region of focal adhesion kinase is a four-helix bundle that binds paxillin. Nat. Struct. Biol. *9*, 101–106.

Heisterkamp, N., Voncken, J.W., Senadheera, D., Gonzalez-Gomez, I., Reichert, A., Haataja, L., Reinikainen, A., Pattengale, P.K., and Groffen, J. (2000). Reduced oncogenicity of p190 Bcr/Abl F-actin-binding domain mutants. Blood *96*, 2226–2232.

Henderson, B.R., and Eleftheriou, A. (2000). A comparison of the activity, sequence specificity, and CRM1-dependence of different nuclear export signals. Exp. Cell Res. *256*, 213–224.

Holmes, K.C., Popp, D., Gebhard, W., and Kabsch, W. (1990). Atomic model of the actin filament. Nature *347*, 44–49.

Hu, J., and Bax, A. (1997). χ_1 angle information from a simple two-dimensional NMR experiment that identifies trans $^3J_{NC\gamma}$ couplings in isotopically enriched proteins. J. Biomol. NMR *9*, 323–328.

Kadlec, J., Izaurralde, E., and Cusack, S. (2004). The structural basis for the interaction between nonsense-mediated mRNA decay factors UPF2 and UPF3. Nat. Struct. Mol. Biol. *11*, 330–337.

Klebe, C., Bischoff, F.R., Ponstingl, H., and Wittinghofer, A. (1995). Interaction of the nuclear GTP-binding protein Ran with its regulatory proteins RCC1 and RanGAP1. Biochemistry *34*, 639–647.

Kubinowa, H., Grzesiek, S., Delaglio, F., and Bax, A. (1994). Measurement of HN-Hα J-couplings in calcium-free calmodulin using new 2D and 3D water-flip-back methods. J. Biomol. NMR *4*, 871–878.

Kutay, U., Bischoff, F.R., Kostka, S., Kraft, R., and Gorlich, D. (1997). Export of importin alpha from the nucleus is mediated by a specific nuclear transport factor. Cell *90*, 1061–1071.

Laskowski, R.A., Rullmannn, J.A., MacArthur, M.W., Kaptein, R., and Thornton, J.M. (1996). AQUA and PROCHECK-NMR: programs for checking the quality of protein structures solved by NMR. J. Biomol. NMR *8*, 477–486.

Lerche, M.H., Meissner, A., Poulsen, F.M., and Sorensen, O.W. (1999). Pulse sequences for measurement of one-bond (15)N-(1)H coupling constants in the protein backbone. J. Magn. Reson. *140*, 259–263.

McWhirter, J.R., and Wang, J.Y. (1991). Activation of tyrosine kinase and microfilament-binding functions of c-abl by bcr sequences in bcr/abl fusion proteins. Mol. Cell. Biol. *11*, 1553–1565.

McWhirter, J.R., and Wang, J.Y. (1993). An actin-binding function

contributes to transformation by the Bcr-Abl oncoprotein of Philadelphia chromosome-positive human leukemias. EMBO J. *12*, 1533–1546.

McWhirter, J.R., Galasso, D.L., and Wang, J.Y. (1993). A coiled-coil oligomerization domain of Bcr is essential for the transforming function of Bcr-Abl oncoproteins. Mol. Cell. Biol. *13*, 7587–7595.

Mingot, J.M., Bohnsack, M.T., Jakle, U., and Gorlich, D. (2004). Exportin 7 defines a novel general nuclear export pathway. EMBO J. *23*, 3227–3236.

Nagar, B., Hantschel, O., Young, M.A., Scheffzek, K., Veach, D., Bornmann, W., Clarkson, B., Superti-Furga, G., and Kuriyan, J. (2003). Structural basis for the autoinhibition of c-Abl tyrosine kinase. Cell *112*, 859–871.

Nilges, M., and O'Donoghue, S.I. (1998). Ambiguous NOEs and automated NOE assignment. Progr. NMR Spectr. *32*, 107–139.

Puntervoll, P., Linding, R., Gemund, C., Chabanis-Davidson, S., Mattingsdal, M., Cameron, S., Martin, D.M., Ausiello, G., Brannetti, B., Costantini, A., et al. (2003). ELM server: a new resource for investigating short functional sites in modular eukaryotic proteins. Nucleic Acids Res. *31*, 3625–3630.

Raitano, A.B., Whang, Y.E., and Sawyers, C.L. (1997). Signal transduction by wild-type and leukemogenic Abl proteins. Biochim. Biophys. Acta *1333*, F201–F216.

Renshaw, M.W., Capozza, M.A., and Wang, J.Y. (1988). Differential expression of type-specific c-abl mRNAs in mouse tissues and cell lines. Mol. Cell. Biol. *8*, 4547–4551.

Ribbeck, K., and Gorlich, D. (2002). The permeability barrier of nuclear pore complexes appears to operate via hydrophobic exclusion. EMBO J. *21*, 2664–2671.

Ruckert, M., and Otting, G. (2000). Alignment of biological macromolecules in novel nonionic liquid crystalline media for NMR experiments. J. Am. Chem. Soc. *122*, 7793–7797.

Sawyers, C. (2004). Targeted cancer therapy. Nature *432*, 294–297.

Smith, K.M., Yacobi, R., and Van Etten, R.A. (2003). Autoinhibition of Bcr-Abl through its SH3 domain. Mol. Cell *12*, 27–37.

Steelman, L.S., Pohnert, S.C., Shelton, J.G., Franklin, R.A., Bertrand, F.E., and McCubrey, J.A. (2004). JAK/STAT, Raf/MEK/ERK, PI3K/Akt and BCR-ABL in cell cycle progression and leukemogenesis. Leukemia *18*, 189–218.

Stuven, T., Hartmann, E., and Gorlich, D. (2003). Exportin 6: a novel nuclear export receptor that is specific for profilin.actin complexes. EMBO J. *22*, 5928–5940.

Taagepera, S., McDonald, D., Loeb, J.E., Whitaker, L.L., McElroy, A.K., Wang, J.Y., and Hope, T.J. (1998). Nuclear-cytoplasmic shuttling of C-ABL tyrosine kinase. Proc. Natl. Acad. Sci. USA *95*, 7457–7462.

Van Etten, R.A., Jackson, P., and Baltimore, D. (1989). The mouse type IV c-abl gene product is a nuclear protein, and activation of transforming ability is associated with cytoplasmic localization. Cell *58*, 669–678.

Van Etten, R.A., Jackson, P.K., Baltimore, D., Sanders, M.C., Matsudaira, P.T., and Janmey, P.A. (1994). The COOH terminus of the c-Abl tyrosine kinase contains distinct F- and G-actin binding domains with bundling activity. J. Cell Biol. *124*, 325–340.

Vigneri, P., and Wang, J.Y. (2001). Induction of apoptosis in chronic myelogenous leukemia cells through nuclear entrapment of BCR-ABL tyrosine kinase. Nat. Med. *7*, 228–234.

Wang, J.Y. (2000). Regulation of cell death by the abl tyrosine kinase. Oncogene *19*, 5643–5650.

Wen, S.T., Jackson, P.K., and Van Etten, R.A. (1996). The cytostatic function of c-Abl is controlled by multiple nuclear localization signals and requires the p53 and Rb tumor suppressor gene products. EMBO J. *15*, 1583–1595.

Wetzler, M., Talpaz, M., Van Etten, R.A., Hirsh-Ginsberg, C., Beran, M., and Kurzrock, R. (1993). Subcellular localization of Bcr, Abl, and Bcr-Abl proteins in normal and leukemic cells and correlation of expression with myeloid differentiation. J. Clin. Invest. *92*, 1925–1939.

Wiesner, S., Hantschel, O., Mackereth, C.D., Superti-Furga, G., and Sattler, M. (2005). NMR assignment reveals an all a-helical fold for the F-actin binding domain of human Bcr-Abl/c-Abl. J. Biomol. NMR, in press.

Wong, S., and Witte, O.N. (2004). The BCR-ABL story: bench to bedside and back. Annu. Rev. Immunol. *22*, 247–306.

Woodring, P.J., Hunter, T., and Wang, J.Y. (2001). Inhibition of c-Abl tyrosine kinase activity by filamentous actin. J. Biol. Chem. *276*, 27104–27110.

Woodring, P.J., Hunter, T., and Wang, J.Y. (2003). Regulation of F-actin-dependent processes by the Abl family of tyrosine kinases. J. Cell Sci. *116*, 2613–2626.

Yoshida, K., Yamaguchi, T., Natsume, T., Kufe, D., and Miki, Y. (2005). JNK phosphorylation of 14–3-3 proteins regulates nuclear targeting of c-Abl in the apoptotic response to DNA damage. Nat. Cell Biol. *7*, 278–285.

Zhang, X., Subrahmanyam, R., Wong, R., Gross, A.W., and Ren, R. (2001). The NH(2)-terminal coiled-coil domain and tyrosine 177 play important roles in induction of a myeloproliferative disease in mice by Bcr-Abl. Mol. Cell. Biol. *21*, 840–853.

Zhu, J., and Wang, J.Y. (2004). Death by Abl: a matter of location. Curr. Top. Dev. Biol. *59*, 165–192.

Accession Numbers

Atomic coordinates have been deposited in the Protein Data Bank under accession number 1ZZP.